Molecular BioSystems

Cite this: *Mol. BioSyst.*, 2011, **7**, 1129–1137

www.rsc.org/molecularbiosystems

PAPER

Mathematical model of PAR1-mediated activation of human platelets†

Leonardo Lenoci,[a] Matthew Duvernay,[a] Shalanda Satchell,[a] Emmanuele DiBenedetto[b] and Heidi E. Hamm*[a]

Received 25th October 2010, Accepted 13th December 2010
DOI: 10.1039/c0mb00250j

Thrombin, one of the major proteases in the coagulation cascade, activates protease activated receptors 1 and 4 (PAR 1 and PAR4) to generate a network of intracellular signals that lead to stable platelet aggregation. Abnormal platelet activation could lead to either thrombosis or bleeding disorders, thus a predictive model of platelet activation would be an invaluable tool for the study of platelet function. In this work, we developed a computational model of PAR1-stimulated human platelet activation fully based on experimental observations. The model is represented by a system of ordinary differential equations (ODEs) describing the kinetics of the interacting components. The model is able to reproduce experimental dose responses and time-courses of cytosolic calcium (Ca^{2+}), phosphatidylinositol 4,5-bisphosphate (PIP2), diacylglycerol (DAG), GTP-bound Ras-proximate-1 (Rap1GTP), secretion of dense-granules, and activation of integrin α2bβ3 (GPIIbIIIa). Because of the inherent complexity of such a model, we also provide a simple way to identify and divide the system into interlinked functional modules to reduce the number of unknown parameters. Both the full and the reduced kinetic models are shown to predict platelet behavior in response to PAR1 activation.

1. Introduction

Thrombosis is one of the major causes of death in the world[1,2] and abnormal platelet activation can lead to either thrombosis or bleeding disorders.[3] Therefore, a predictive model of platelet function that would facilitate the search for risk factors for thrombosis would be a valuable tool. Thrombin, one of the most potent platelet activators, activates protease activated receptors 1 and 4 (PAR1 and PAR4), which are G-protein coupled receptors (GPCRs).[4,5] The dynamics of thrombin signaling to platelet aggregation is very complex, because it involves multiple G proteins, each coupled to a network of signaling pathways, that lead to secretion, feed-forward activation of other GPCRs, integrin activation and subsequent formation of an irreversible platelet aggregate.[4] Although the individual signaling pathways activated by thrombin have been extensively studied in the past years,[4,6–8] how they interconnect and ultimately integrate to lead to platelet aggregation is very important but still largely unknown.

Anomalous platelet aggregation can lead to dangerous thrombotic effects.[3] Current medical therapies to prevent these conditions often include anti-platelet drugs that aim to attenuate platelet activation. Common side effects of these drugs include delayed formation of a platelet aggregate and/or a long duration of action, causing unwanted bleeding complications.[9,10] An important long-term goal of this field is to seek alternative therapeutic routes with fewer collateral effects. Since the signaling pathways downstream of PAR1 and PAR4 are not fully understood, a predictive computational model of the key signaling factors that lead to abnormal platelet activation would help to improve our understanding of the platelet biology and potentially allow for the design of more targeted therapeutic interventions with fewer side effects. To this end, computational models have provided an integrated view of the many interacting metabolites involved in signal transduction,[11,12] helped achieve a better understanding of cell surface receptors,[13,14] and led to the discovery of new molecular interactions.[15] Moreover, models based on accurate experimental data sets are also useful to make experimentally verifiable predictions in cellular signaling.[16]

Besides being of inherent medical and biological importance, platelets also constitute a well-suited model system for computational biologists, because they are readily available from blood donors and lack a nucleus,[4] making it possible to model cell signaling processes without the added complexity introduced by the whole-genome transcriptional regulatory system. Nonetheless, only a few computational studies of platelet signaling have been carried out in the past years, mostly focusing on the response of platelets to adenosine diphosphate (ADP) stimulation.[17,18] In this work, we created an ordinary differential equation (ODE) model, fully based on

[a] *Department of Pharmacology, Vanderbilt University Medical Center, Nashville, TN, USA. E-mail: heidi.hamm@vanderbilt.edu*
[b] *Department of Mathematics, Vanderbilt University, Nashville, TN, USA*

† Electronic supplementary information (ESI) available: Explicit model equations in MATLAB format are in Text S1. See DOI: 10.1039/c0mb00250j

experimental observations, that describes the kinetics of a human platelet in response to PAR1 stimulation. Although the model is far from being exhaustive (for instance, it does not account explicitly for the autocrine feedback mechanism through ADP and thromboxane, although the parameters are chosen so that their effect is implicitly taken into account), it incorporates the kinetics of the major components involved in human platelet signaling, from G_q, $G_{12/13}$ and G_i activation to integrin GPIIbIIIa activation, including phospholipase C and D (PLC, PLD), protein kinase C and B (PKC, PKB/Akt), and Rap1 signaling. The current version of the model is able to reproduce PAR1 dose responses and account for the complex platelet feed-forward and feedback mechanisms that lead to biphasic time-courses[19] and stable platelet aggregation. The simulation results might be of help in identifying those model components that play a crucial role in platelet activity and whose perturbation could predict thrombotic states.

Important differences characterize thrombin signaling from PAR1-AP signaling in human platelets. During coagulation, thrombin produced at the site of injury first cleaves the higher-affinity receptor PAR1 and then activates the lower-affinity receptor PAR4.[4] In the case of the intracellular Ca^{2+} response, this sequential-activation mechanism generates a biphasic signal which has a very rapid ($\sim$30 s) spike due to PAR1 signaling, followed by a much-slower (20–70 fold) and prolonged component that arises from thrombin activation of the lower-affinity PAR4 receptors.[20] Other differences in the signaling of PAR4 and PAR1 have been recently pointed out and include differential regulation of the protease-activated receptors in irreversible platelet aggregation,[21] differences in the phosphoinositide-3 kinase signaling axis[22] and in the phosphatidic acid-dependent pathways.[23] Additionally, PAR4, but not PAR1 signaling participates in human platelet aggregation *via* Ca^{2+} mobilization and synergistic P2Y12 receptor activation.[24]

Because of the complexity of the system, accurate computational models must inevitably carry a large number of parameters, and the consequent unwieldiness and poor computational stability.[25–27] In this study, we also propose a simple way to identify functional modules (or sub-networks)[27] and reduce the number of model parameters only to those that dramatically affect PAR1 signaling. Both the full and the reduced ODE models are able to predict platelet behavior in response to PAR1 activation.

2. Model and methods

The model captures the kinetics of the major signaling pathways induced by PAR1 in human platelets. Reaction schemes and constants used in the simulations were either adapted from existing computational models[17,18,28–30] or estimated using the least-squares fitting method[31] to fit both literature values and experimental data. The full model is currently populated with 60 ODEs (excluding the equations that regulate cytosolic Ca^{2+} mobilization, which are described in detail elsewhere[32]) derived from the reaction schemes in Table 1 according to the law of mass action. The reaction schemes of Table 1 and their constants are to be considered here as "effective", because they intrinsically account for the kinetics of a large number of biological processes. A pictorial representation of the major PAR1-induced pathways in platelets is given in Fig. 1.

The system of ODEs was integrated over a time period of 800 s on a MATLAB (R2009b, The Mathworks, Natick, MA) platform using the ODE15s solver. The initial concentrations (see Table 2) of the metabolites were chosen to be in agreement with known resting platelet values[4] and/or with recent theoretical estimations based on steady-state kinetic modeling of platelet activation by ADP.[18]

Human platelets were obtained from healthy volunteers within the Vanderbilt University community. Studies were approved by the Vanderbilt University Institutional Review Board. Informed consent was obtained from all individuals before blood donation. Blood samples were centrifuged at 170*g* for 15 min at room temperature, after which platelet-rich plasma was transferred into a conical tube containing a 10% acid citrate dextrose solution (39 mM citric acid, 75 mM sodium citrate, and 135 mM glucose, pH 7.4) and centrifuged at 800*g* for 10 min at room temperature. Platelets were resuspended in Tyrode's buffer (12 mM $NaHCO_3$, 127 mM NaCl, 5 mM KCl, 0.5 mM NaH_2PO_4, 1 mM $MgCl_2$, 5 mM glucose, and 10 mM HEPES), and the final platelet concentration was adjusted after counting using a Coulter counter (Beckman Coulter, Fullerton, CA) as indicated. Platelets were activated with 20 μM of the specific PAR1 agonist SFLLRN and all experiments were performed as described previously.[21,24] The data reported here were obtained using washed platelets from at least three different subjects.

2.1 PAR1 signaling overview

Upon platelet stimulation by a specific PAR1 agonist, PAR1, simultaneously activates three classes of G proteins: G_q, G_i, and $G_{12/13}$.[5] The α subunit of the G_q protein activates the β isoforms of phospholipase C (PLCβ), which hydrolyze the lipid phosphatidylinositol 4,5-bisphosphate (PIP2) to generate the second messengers inositol 1,4,5-trisphosphate (IP3) and diacylglycerol (DAG).[33] Then, IP3 regulates the activity of the inositol trisphosphate receptors (IP_3R) on the surface of the platelet dense tubular system (DTS), allowing the rapid release of Ca^{2+} into the cytoplasm.[4,32]

Both DAG and the rise in cytosolic Ca^{2+} concentration modulate the activity of protein kinase C (PKC).[4,28] Following platelet stimulation, the α subunit of the $G_{12/13}$ protein activates the small GTPase RhoA that, along with PKC and PIP2, stimulates the enzyme phospholipase D1 (PLD1), which catalyzes the formation of phosphatidic acid (PA) from phosphatidyl choline (PC).[34–37] PA, which is converted into DAG by phosphatidic acid phosphatase (PAP), is also known to be one of the major regulators of PI5K,[38,39] the kinase that phosphorylates PIP into PIP2. Moreover, a recent study reported that the subunit $G_{13}\alpha$ can bind directly to integrin GPIIbIIIa to mediate "outside-in" signaling.[40] Activated Rho GTPase is also known to promote platelet cytoskeletal changes following stimulation.[41]

Ca^{2+} and DAG signaling is integrated by CalDAG-GEFI into the activation of the small GTPase Rap1, by promoting the release of GDP and the loading of GTP.[42,43] Rap1 is then

Table 1 Symbolic reaction schemes and effective kinetic parameters used in the simulation of a PAR1-stimulated human platelet

Symbolic reactions	k_1	k_{-1}	Ref.
Reactions governing PAR1 activation			
Agonist + PAR1 $\rightleftharpoons$ PAR1*	7.50×10^4 M^{-1} s^{-1}	1.00×10^{-3} s^{-1}	56
Agonist $\rightarrow$ null	2.00×10^{-1} s^{-1}		29
PAR1* $\rightarrow$ null	2.00×10^{1} s^{-1}		29
Reactions governing G_q activation			
PAR1* + $G_qGDP{\cdot}\beta\gamma$ $\rightleftharpoons$ PAR1*·$G_qGDP{\cdot}\beta\gamma$	1.00×10^8 M^{-1} s^{-1}	1.00 s^{-1}	57
PAR1*·$G_qGDP{\cdot}\beta\gamma$ $\rightleftharpoons$ PAR1*·$G_q{\cdot}\beta\gamma$ + GDP	5.00 s^{-1}	1.00×10^6 M^{-1} s^{-1}	57
PAR1*·$G_q{\cdot}\beta\gamma$ + GTP $\rightleftharpoons$ PAR1*·$G_qGTP{\cdot}\beta\gamma$	1.00×10^6 M^{-1} s^{-1}	1.00×10^{-1} s^{-1}	57
PAR1*·$G_qGTP{\cdot}\beta\gamma$ $\rightleftharpoons$ PAR1* + G_qGTP + $\beta\gamma$	2.00 s^{-1}	1.00×10^7 M^{-2} s^{-1}	57
$G_qGTP \rightarrow G_qGDP$	2.00×10^{-2} s^{-1}		58–60
Reactions governing IP3 and DAG generation			
PLCβ + G_qGTP $\rightleftharpoons$ PLCβ·G_qGTP	5.00×10^8 M^{-1} s^{-1}	5.00 s^{-1}	60,61
PLCβ·$G_qGTP \rightarrow$ PLCβ·G_qGDP	1.5×10^{1} s^{-1}		59,60
PLCβ·$G_qGDP \rightleftharpoons$ PLCβ + G_qGDP	1.00×10^5 s^{-1}	1.00×10^2 M^{-1} s^{-1}	62
PLCβ·G_qGTP + PIP2 $\rightleftharpoons$ PLCβ·G_qGTP·PIP2	1.00×10^9 M^{-1} s^{-1}	1.00 s^{-1}	62
PLCβ·G_qGTP·PIP2 $\rightarrow$ PLCβ·G_qGTP + IP3/DAG	3.20×10^2 s^{-1}		62
IP3 $\rightarrow$ null	1.70×10^{-2} s^{-1}		29
Reactions governing Ca^{2+} mobilization			
As described previously			See Table S1 and Text S1 (ESI†)[32]
Reactions governing $G_{12/13}$ activation			
PAR1* + $G_{12/13}GDP{\cdot}\beta\gamma$ $\rightleftharpoons$ PAR1*·$G_{12/13}GDP{\cdot}\beta\gamma$	1.00×10^8 M^{-1} s^{-1}	1.00 s^{-1}	57
PAR1*·$G_{12/13}GDP{\cdot}\beta\gamma$ $\rightleftharpoons$ PAR1*·$G_{12/13}{\cdot}\beta\gamma$ + GDP	5.00 s^{-1}	1.00×10^6 M^{-1} s^{-1}	57
PAR1*·$G_{12/13}{\cdot}\beta\gamma$ + GTP $\rightleftharpoons$ PAR1*·$G_{12/13}GTP{\cdot}\beta\gamma$	1.00×10^6 M^{-1} s^{-1}	1.00×10^{-1} s^{-1}	57
PAR1*·$G_{12/13}GTP{\cdot}\beta\gamma$ $\rightleftharpoons$ PAR1* + $G_{12/13}GTP$ + $\beta\gamma$	2.00 s^{-1}	1.00×10^7 M^{-2} s^{-1}	57
$G_{12/13}GTP \rightarrow G_{12/13}GDP$	4.00×10^{-3} s^{-1}		63,64
Reactions governing Rho activation			
GEF_{Rho} + $G_{12/13}GTP$ $\rightleftharpoons$ $GEF_{Rho}{\cdot}G_{12/13}GTP$	1.00×10^9 M^{-1} s^{-1}	3.00 s^{-1}	60
$GEF_{Rho}{\cdot}G_{12/13}GTP \rightarrow GEF_{Rho}{\cdot}G_{12/13}GDP$	1.00×10^{-2} s^{-1}		63
$GEF_{Rho}{\cdot}G_{12/13}GDP \rightleftharpoons GEF_{Rho}$ + $G_{12/13}GDP$	1.00×10^6 s^{-1}	3.00 M^{-1} s^{-1}	29
$GEF_{Rho}{\cdot}G_{12/13}GTP$ + RhoGDP $\rightleftharpoons$ $GEF_{Rho}{\cdot}G_{12/13}GTP$·RhoGDP	7.70×10^9 M^{-1} s^{-1}	7.70×10^2 s^{-1}	29
$GEF_{Rho}{\cdot}G_{12/13}GTP$·RhoGDP $\rightarrow$ $GEF_{Rho}{\cdot}G_{12/13}GTP$ + RhoGTP	1.03×10^4 s^{-1}		29
RhoGTP $\rightarrow$ RhoGDP	6.00×10^{-2} s^{-1}		65
Reactions governing G_i activation			
PAR1* + $G_iGDP{\cdot}\beta\gamma$ $\rightleftharpoons$ PAR1*·$G_iGDP{\cdot}\beta\gamma$	1.00×10^8 M^{-1} s^{-1}	1.00 s^{-1}	57
PAR1*·$G_iGDP{\cdot}\beta\gamma$ $\rightleftharpoons$ PAR1*·$G_i{\cdot}\beta\gamma$ + GDP	5.00 s^{-1}	1.00×10^6 M^{-1} s^{-1}	57
PAR1*·$G_i{\cdot}\beta\gamma$ + GTP $\rightleftharpoons$ PAR1*·$G_iGTP{\cdot}\beta\gamma$	1.00×10^6 M^{-1} s^{-1}	1.00×10^{-1} s^{-1}	57
PAR1*·$G_iGTP{\cdot}\beta\gamma$ $\rightleftharpoons$ PAR1* + G_iGTP + $\beta\gamma$	2.00 s^{-1}	1.00×10^7 M^{-2} s^{-1}	57
$G_iGTP \rightarrow G_iGDP$	4.00×10^{-3} s^{-1}		66
Reactions governing PKB/Akt activation			
βγ + Akt $\rightleftharpoons$ Akt*	1.00×10^5 M^{-1} s^{-1}	1.00 s^{-1}	
Reactions governing PKC activation			
$Ca^{2+} + PKC \rightleftharpoons PKC^*_{Ca}$	0.60×10^4 M^{-1} s^{-1}	0.50 s^{-1}	28
$DAG + PKC \rightleftharpoons PKC^*_{DAG}$	0.008×10^4 M^{-1} s^{-1}	8.6348 s^{-1}	28
Reactions governing PLD activation			
$PKC^*_{Ca} + PLD \rightleftharpoons PLD^*_{PKC{\cdot}Ca}$	1.00 M^{-1} s^{-1}	1.00×10^4 s^{-1}	34–37
$PKC^*_{DAG} + PLD \rightleftharpoons PLD^*_{PKC{\cdot}DAG}$	1.00×10^2 M^{-1} s^{-1}	1.00 s^{-1}	34–37
$PIP2 + PLD \rightleftharpoons PLD^*_{PIP2}$	1.00×10^3 M^{-1} s^{-1}	1.00 s^{-1}	34–37
Reactions governing PLD activity			
PI5K* $\rightleftharpoons$ PIP2	1.00 s^{-1}	1.00 s^{-1}	See Section 3.2
PA $\rightleftharpoons$ DAG	1.00 s^{-1}	0.20×10^{-1} s^{-1}	See Section 3.3
Reactions governing Rap1 activation			
CalDAG-GEF + DAG + Ca^{2+} $\rightleftharpoons$ CalDAG-GEF*	2.00×10^{10} M^{-1} s^{-2}	1.50×10^{-3} s^{-1}	42
CalDAG-GEF* + Rap1GDP $\rightleftharpoons$ CalDAG-GEF*·Rap1GDP	7.70×10^9 M^{-1} s^{-1}	7.70×10^2 s^{-1}	
CalDAG-GEF*·Rap1GDP $\rightarrow$ CalDAG-GEF* + Rap1GTP	1.03×10^4 s^{-1}		
Rap1GTP $\rightarrow$ Rap1GDP	6.00×10^{-2} s^{-1}		
Akt* + Rap1GDP $\rightleftharpoons$ $Rap1GTP_{Akt*}$	1.00×10^5 M^{-1} s^{-1}	0.70×10^{-2} s^{-1}	
Reactions governing integrin activation			
Rap1GTP + RIAM $\rightleftharpoons$ Rap1GTP·RIAM	1.00×10^9 M^{-1} s^{-1}	3.00 s^{-1}	44
Rap1GTP·RIAM + TALIN $\rightleftharpoons$ Rap1GTP·RIAM·TALIN	5.00×10^8 M^{-1} s^{-1}	5.00 s^{-1}	44
Rap1GTP·RIAM·TALIN + GPIIbIIIa $\rightleftharpoons$ GPIIbIIIa*	1.00×10^3 M^{-1} s^{-1}	1.50×10^{-3} s^{-1}	44
Reactions governing exocytosis			
Ca^{2+} + PKC* $\rightarrow$ ATP	1.20×10^5 M^{-1} s^{-1}		See Section 3.5
ATP $\rightarrow$ null	1.86×10^{-3} s^{-1}		See Section 3.5

implicated, *via* its downstream effector RIAM, in the activation of integrin GPIIbIIIa.[44–46] The $G_i\beta\gamma$ subunit mediates the activation of the isoform γ of phosphatidylinositol kinase (PI3K) that phosphorylates PIP2 to generate the lipid second messenger PIP3. The role of PIP3 in platelets is still not fully understood,[47] but it is thought that PIP3 leads to the

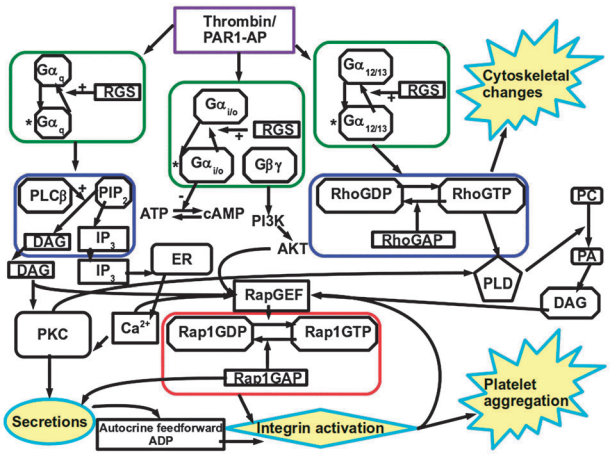

Fig. 1 Schematic of PAR1-mediated signaling in a human platelet. The colored boxes represent putative modules. PIP2 indicates phosphatidylinositol 4,5-bisphosphate; DAG diacylglycerol; PLD phospholipase D1, PA phosphatidic acid; PC phosphatidyl choline; PKC protein kinase C; Akt protein kinase B; PI3K and PI5K phosphoinositide 3 and 5 kinases; Rho GTPase; Rap1 Ras-proximate-1; GDP and GTP guanine di-and-triphospate. RGS indicates the regulators of GTP hydrolysis.

Table 2 Initial metabolite concentrations used in the simulation of a PAR1-stimulated human platelet.

Species	Concentrations	Ref.
SFLLRN	20.00×10^{-6} M	
PAR1	6.00×10^{-9} M	29
G_qGDP·βγ	4.30×10^{-9} M	18,29
GTP	1.00×10^{-6} M	18,29
PLCβ	3.00×10^{-9} M	18,29
PIP2	200×10^{-6} M	4
IP3	5.00×10^{-9} M	4
Ca^{2+}	5.50×10^{-8} M	4
$G_{12/13}$GDP·βγ	4.30×10^{-9} M	29
RhoGDP	3.00×10^{-9} M	29
RhoGEF	3.00×10^{-9} M	29
PKC	30.00×10^{-6} M	18
$PKC^{Ca^{2+}}$	2.00×10^{-8} M	18
DAG	1.00×10^{-8} M	4
PLD	10.00×10^{-6} M	36,37
PA	1.00×10^{-8} M	36,37
G_iGDP·βγ	4.30×10^{-9} M	66
CalDAG-GEFI	3.00×10^{-9} M	42,43
Rap1GDP	3.00×10^{-9} M	44
RIAM	1.00×10^{-9} M	44
TALIN	1.00×10^{-9} M	44
GPIIbIIIa	10.00×10^{-6} M	44
Akt	3.00×10^{-9} M	

activation of PKB/Akt. Experimental data also suggest a potential role for Akt in the activation of Rap1.[21]

2.2 Platelet exocytosis

Platelet granule secretions mediate blood coagulation and promote wound healing.[4,48–50] Exocytosis also plays an important role in vascular diseases, for instance by accelerating the formation of arteriosclerotic lesions.[4,48–50] Recent platelet studies have shown that an increased platelet secretion is present in humans with different vascular pathologies, such as hypertension, peripheral artery disease and coronary artery disease.[4,48–50] Platelets contain three types of secretory organelles with different molecular content and kinetics of exocytosis: dense-granules, α-granules and lysosomes.[4] There are about 80 α-granules per human platelet and nearly 10-fold fewer dense-granules.[4] While dense-granules contain high concentrations of low molecular weight compounds that amplify platelet activation, such as adenosin diphosphate (ADP), serotonin, and calcium, α-granules carry large polypeptides such as fibrinogen, von Willebrand factor (vWf) and several coagulation factors and co-factors.[4] However, it has recently been shown that α- and dense-granules might also carry a similar molecular cargo. Detectable amounts of integrin α2bβ3 and P-selectin have, in fact, been found in both α- and dense-granules.[49,51]

Platelet exocytosis occurs through mechanisms similar to those taking place in neurons, which involve the movement of granules near the plasma membrane, their fusion with it, and the subsequent release of the intracellular contents.[4,48–51] The secretory events are mediated by *N*-ethylmaleimide-sensitive factor attachment protein receptors (SNAREs) that can either be associated with granules (vSNAREs) or associated with target membranes (tSNAREs). Membrane fusion occurs upon association of the vSNAREs with their cognate tSNAREs. Known platelet vSNAREs include VAMP-2,-3,-7, and -8, whereas known platelet tSNAREs include syntaxins 2, 4, 7, and 11 and SNAP-23,-25, and -29.[4,51] The function of SNAREs in exocytosis is tightly regulated by Sec/Munc (SM) proteins in order to prevent indiscriminant secretion. Known platelet SM proteins include Munc13-4 and Munc18a, b, and c.[4,51,52] In inactivated platelets, Munc18c is primarily found in complex with syntaxin-4 indicating that Munc18c serves as a negative regulator of SNAREs function.[4,48,52] Several other chaperone proteins that directly interact with the SNAREs and mediate their function have been also described in platelets.[4,51] Among these, NSF is a hexameric ATPase whose primary role is to disassemble SNARE complexes present on the same membrane (*cis*-conformation) to make them available for interaction with their cognate SNAREs on opposing membranes (*trans* conformation). NSFs are bound and activated by the soluble NSF-attachment proteins (SNAPs).[48] Lipid components such as phosphatidic acid (PA) and 4,5-bisphosphate (PIP2) have also been studied in platelet secretion and been associated to membrane fusion.[4,53]

Following platelets activation by a specific ligand such as thrombin and ADP, intracellular [Ca^{2+}] increases to micro-molar levels thus triggering exocytosis.[4,49,51] Although increases in intracellular [Ca^{2+}] are sufficient to induce secretion, PKC has also been shown to act synergistically with [Ca^{2+}] to amplify secretions.[4,48–51] Recent studies have shown that inhibition of active PKC can block platelet secretion.[4,48–51] Unfortunately, the mechanisms by which increases of intracellular [Ca^{2+}] are coupled to exocytosis are still unclear.[4,49,51,53] On the other hand, recent studies have hinted a precise role for PKC in exocytosis.[4,49,51] The regulation of the interactions between SNARE proteins occurs through PKC-dependent phosphorylation events. Upon platelet stimulation, PKC phosphorylates Munc18c and syntaxin-4

thus reducing Munc18 affinity to syntaxins and inhibiting syntaxin-4 binding to SNAP-23.[53,54]

2.3 Modules

Biological networks can often be very complex to model, because they involve a large number of components and pathways. A well known technique to avoid the cumbersomeness of these intricate systems consists in subdividing the whole signaling network into functional sub-networks (or modules) with common input and output signals. A pictorial representation of the putative modules is given in Fig. 1. The modules are then studied separately and at last joined to create a sound model able to reproduce the experimental data.[27]

To identify functional modules and relevant model parameters, we organized kinetic constants into a pseudo-coefficient matrix where the rows represent the ODEs and the columns the metabolites. In the 60 × 60 matrix, of which a symbolic cartoon is reproduced in Fig. 2, a small variation of the constants along the diagonal and in its near proximity affected the simulation results (*e.g.* Ca^{2+} time-course) dramatically. On the other hand, our simulations show that the constants far from the diagonal can be safely neglected (or modified) without qualitatively affecting the results. On the basis of these considerations, we subdivided the system into interlinked signaling modules (see Fig. 1) and reduced the number of parameters accordingly. In Fig. 5C and D we report Ca^{2+} mobilization curves for the full and the reduced kinetic models. No appreciable differences were found between the two result sets. We stress how modularization in conjunction with sensitivity analysis methods[55] can help reduce dramatically the number of model parameters and therefore its complexity. A study assessing the numerical stability and sensitivity of the present model to parameter values is currently in progress and will be the subject of a future publication.

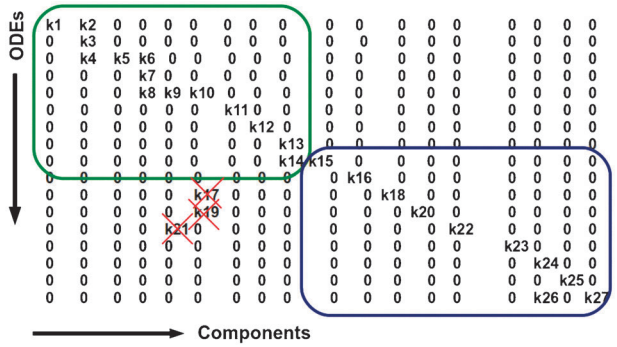

Fig. 2 Symbolic representation of a portion of the pseudo-coefficient matrix of the ODE system. The colored boxes represent putative modules and the crossed elements were shown not to affect the simulation results.

3. Results

Due to the complexity of the large number of processes that regulate platelet activation, a fully-detailed model of platelet signaling would be extremely difficult to generate and computationally untreatable. In this study, we propose a computational model fully based on experimental observations that captures only the essential features of PAR1-mediated signaling by leaving out many details. This approach presents two advantages: the reduction of the model complexity (*i.e.* number of equations and parameters) and the ability to identify those model components that might play a crucial role in abnormal platelet activity, with the ultimate goal of pinpointing key processes. These processes might then point toward loci for risk factor-generating genetic variation, and new therapeutic targets.

3.1 Cytosolic calcium mobilization

Upon platelet stimulation, IP3 concentration levels increase quickly (~30 s) as a result of PIP2 hydrolysis. The rise of IP3 concentration triggers the opening of the IP_3R channels on the surface of the DTS, leading to the fast release of calcium ions into the cytoplasm through well-understood mechanisms.[17,32] For platelets stimulated with 20 μM of PAR1-AP, our model predicts a 2.3-fold increase (Fig. 3B) in levels of cytosolic calcium, which corresponds to a peak value of 126.5 nM (Fig. 3A). Fig. 3A and B report simulated calcium transients for concentrations of PAR1-AP in the range 0 to 20 μM. In Fig. 4A, we show experimental (blue) and simulated (red)

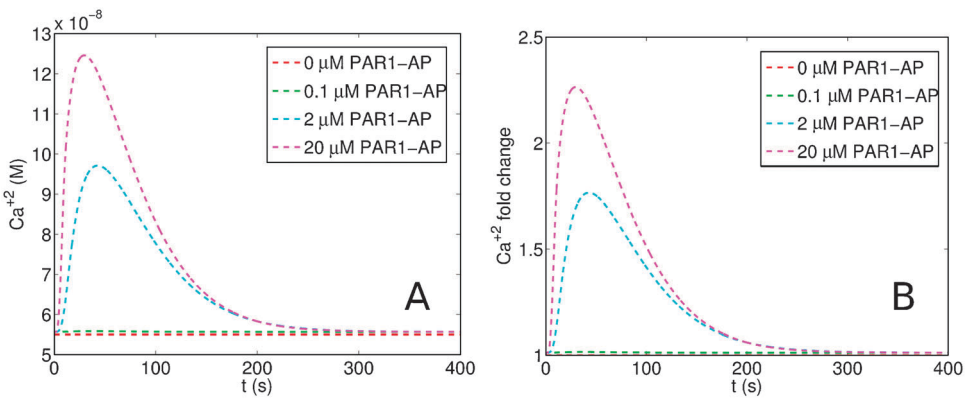

Fig. 3 (A) Simulated Ca^{2+}-mobilization transients in real units and (B) simulated Ca^{2+}-mobilization transients in fold-change units for platelets stimulated by 0, 0.1, 2, and 20 μM of PAR1-AP. The simulation results predict a 2.3-fold increase in intracellular Ca^{2+} concentration in human platelets stimulated with 20 μM of agonist peptide.

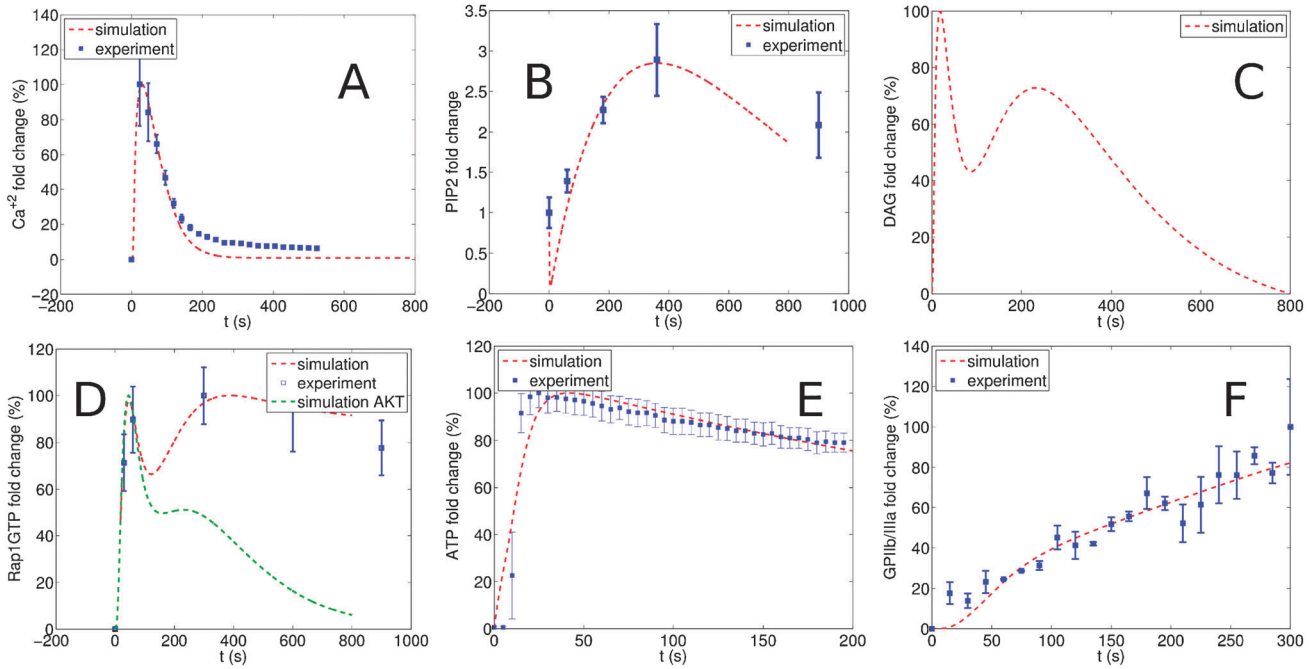

Fig. 4 Experimental and simulated (A) Ca^{2+}, (B) PIP2, and (D) Rap1 time-courses in platelets stimulated with 20 μM of PAR1 agonist peptide. (C) Simulated DAG time-course. (E) Experimental and simulated ATP and (F) GPIIbIIIa time-courses. Units are normalized as percentages due to inherently different basal levels in each blood donor. The normalization is calculated using the expression fold change $= \frac{y-\min(y)}{\max(y)-\min(y)} \times 100$.

Ca^{2+} responses in human platelets stimulated with 20 μM of SFLLRN as described in ref. 24. We used fold-change units expressed in percentages, because blood from three different donors was used in the experiments and each donor had different basal levels. Fig. 5A and B show simulated and experimental dose responses of Ca^{2+} and GPIIb/IIIa. In the case of the calcium responses, our simulations predict an EC_{50} = 1.64 μM, consistent with the experimental value EC_{50} = 1.6 μM and with a recent experimental estimation reported by Covic *et al.* (EC_{50} = 1.8 ± 0.5 μM).[20] The simulated curves were obtained by adapting the calcium-mobilization model for Purkinje cells proposed by Keizer

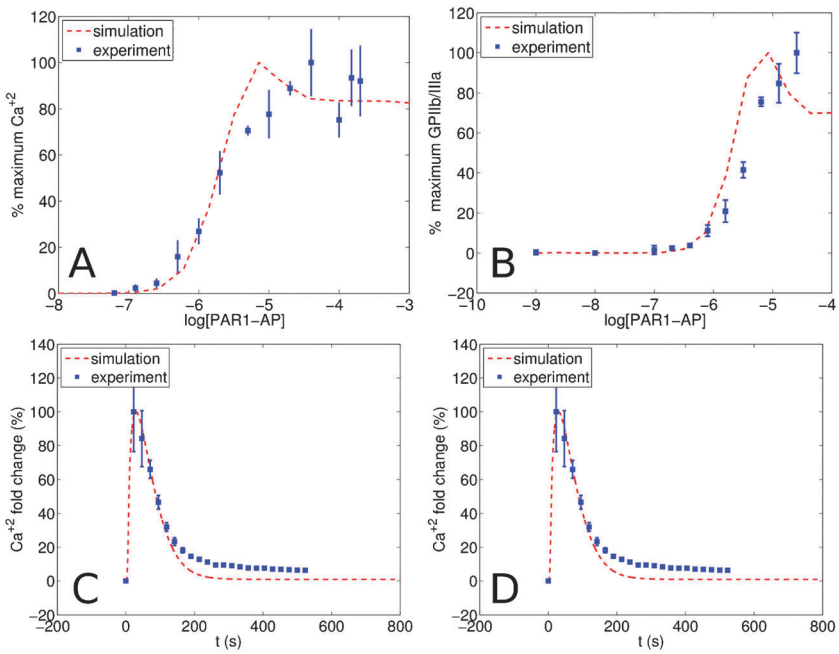

Fig. 5 Experimental (EC_{50} = 1.6 μM) and simulated (EC_{50} = 1.64 μM) dose responses for (A) Ca^{2+} and (B) GPIIbIIIa. Simulated Ca^{2+} transients in the reduced (C) and the full (D) kinetic models. Both simulated and experimental calcium dose responses EC_{50} are consistent with previously reported experimental estimations.[20]

and De Young[32] to fit the experimental data in platelets. In this model, IP3/Ca^{2+} channels are thought to be composed of four identical subunits of which only three are independently involved in the transport of Ca^{2+} ions. Each subunit is then assumed to be composed of one IP3 binding site and two Ca^{2+} binding sites. Each subunit can therefore exist in eight different states denoted $S_{i_1 i_2 i_3}$ with transitions regulated by second-order (a_i) and first-order (b_i) rate constants and the coefficients i_j assuming the values 0 (unoccupied) or 1 (occupied). Assuming that the binding site i_1 is the IP3 binding site and that i_2 and i_3 are the calcium activation and inactivation sites, respectively, only state S_{110} contributes to ion transport. Furthermore, all three subunits must be in this state in order for the channel to be open. Detailed equations describing the dynamics of a subunit are reported in ref. 32. A comparison between the parameters used in ref. 32 and those used in the simulations is given in Table S1 (ESI†). It is worth noting that the present model does not consider all the mechanisms that govern platelet activation, thus the small discrepancies between experimental and simulated results can be attributed to this fact.

3.2 Phosphatidylinositol 4,5-bisphosphate

In stimulated platelets, PIP2 concentration levels are determined by PLCβ and PI5K activities *via* opposite mechanisms. Rapidly after platelet stimulation, PLCβ hydrolyzes PIP2 to produce the second messengers IP3 and DAG. Then, PI5K phosphorylates PIP to replenish the platelets with PIP2. The latter event occurs on a much slower time scale (~300 s) in comparison to the former and it is thought to involve complex feed-forward and feedback mechanisms.[38,39]

The regulation of PI5K in platelets is poorly understood, but there is increasing evidence to suggest that PA and ADP-ribosylation factor (Arf) could play an important role in its activation.[38,39] PA concentration levels are strongly regulated by the activity of PLD1, of which Arf is one of the activators.[35] Interestingly, PI5K itself is regulated by Arf, but Arf regulation and role in platelets is still mostly unclear.[38,39,67] For these reasons, a fully-detailed kinetic model of PI5K regulation would require the formulation of too many hypothetical reaction schemes with the introduction of a large number of unknown parameters, most of which cannot be validated experimentally. Thus, we have measured the time-course of PIP2 formation in PAR1-activated platelets[21] and sought a mathematical model that could fit those data. We assumed that the time-course of the activated form of PI5K could be calculated using the equation below

$$[\mathrm{PI5K^*}] = At\exp(-Bt), \quad (1)$$

where A and B are fitting constants and t is the time. In this equation, the parameters $A = 4.30\ \mu M\ s^{-1}$ and $B = 2.78 \times 10^{-3}\ s^{-1}$ were estimated to fit our experimental measurements of PI5K and PIP2 time-courses reported in ref. 21. Simulated PIP2 transients were obtained by inserting eqn (1) in the reaction schemes of Table 1.

Fig. 4B shows experimental (blue)[21] and simulated (red) PIP2 time-courses in human platelets stimulated with 20 μM of SFLLRN as described in detail in ref. 21. Interestingly, the simulated curve suggests that PIP2 regulation occurs in two distinct phases. The first part of the curve exhibits a steep decrease of concentration, because of PLC activity. This phenomenon is very fast and, at short times (first ~10 s from stimulation), prevails on the production of PIP2 by PI5K activity. At long times ($t > 10$ s), the PI5K-mediated production of PIP2 occurs at a higher rate than the depletion caused by PLC activity, resulting in an increase of concentration up to ~3 fold more than the control value. We note that the initial PIP2 consumption was too fast to be captured in our experiments.[21]

3.3 Diacylglycerol

Previous studies have revealed that thrombin-stimulated platelets exhibit multiphasic increases in diacylglycerol levels.[19] These data are suggestive of more than one source of diacylglycerol in platelets. The primary sources of DAG are PIP2 hydrolysis and phosphatidic acid phosphatase (PAP). On the basis of our previous observations of the regulation of PI5K, it appears logical to assume that, upon platelet stimulation, the PA time-course could be calculated as follows

$$[\mathrm{PA}] = Ct\exp(-Dt), \quad (2)$$

where $C = 52.0\ pM\ s^{-1}$ and $D = 6.67 \times 10^{-3}\ s^{-1}$ are fitting constants, and t is the time. We note that PA levels in activated platelets are extremely difficult to measure, because the signaling lipid is rapidly converted into other products. Instead, the addition of a butyl alcohol (*i.e.* 1-butanol) alters PLD activity and is a preferred substrate, primarily forming phosphatidyl butanol (P-butanol), which is not a signaling molecule and therefore can be measured. Recent studies of PAR1-stimulated platelets show only a small fold-change in the levels of P-butanol following activation[68] suggesting that PIP2 hydrolysis should account for the greater contribution to DAG levels. In Fig. 4C we show the simulated biphasic DAG time-course with the larger contribution (first peak) attributable to PIP2 hydrolysis.

3.4 Ras-proximate-1 and integrin activation

Rap1, a Ras family member, is highly expressed in human platelets. Once in its GTP-bound form, it integrates the signals of the G_q, $G_{12/13}$ and G_i proteins to induce integrin activation and subsequent platelet aggregation. The GDP–GTP exchange is thought to occur primarily by means of the specific guanine exchange factor CalDAG-GEFI. CalDAG-GEFI is known to transduce Ca^{2+} and DAG signaling to activate Rap1.[42,43] One of our recent studies has shown that PAR1-mediated Rap1 activity is sensitive to agents that perturb PI-kinase and Akt signaling.[21] Both platelets treated with the potent PI3K inhibitor LY294002 and the Akt inhibitor Akt X showed a significantly attenuated Rap1 response relative to control conditions, suggesting the presence of alternative Rap1 activation mechanisms. In this work, we simulated both the control and the perturbed platelet conditions to test our model against the experimental data. For instance, Akt X conditions were simulated by tuning down the output of the Akt signaling module. In Fig. 4D we show the experimental (blue)[21] and the simulated Rap1 time-courses in untreated platelets (red) along with the Rap1 response in platelets treated with Akt X

(green).[21] The simulated results show that Akt X-treated platelets present an attenuated Rap1 signal in agreement with the experimental data.

Activated Rap1 promotes the activation of the integrin complex GPIIbIIIa through its downstream effector RIAM *via* mechanisms described in ref. 44. Upon activation, integrin GPIIbIIIa undergoes a structural change that allows it to interact with the ligand fibrin in the extracellular matrix, leading to aggregation. Simulated and experimental integrin time-courses are shown in Fig. 4F, respectively, in red and blue colors.

3.5 Exocytosis

Due to the high complexity of the molecular events underlying platelet exocytosis, we created a mathematical module that describes platelet dense-granule secretion by explicitly taking into account only the contribution of Ca^{2+} and PKC signaling. The model is fully based on experimental observations and leaves out all the molecular details involved in platelet secretion. In a similar fashion to a previously published model of exocytosis in neuroendocrine cells,[69] we summarized the kinetic processes underling ATP secretion by means of the two-step symbolic reaction scheme:

$$[Ca^{2+}] + [PKC^*] \rightarrow^{k_1} [ATP] \rightarrow^{k_2} \text{null}, \qquad (3)$$

where k_1 is the effective rate of exocytosis and k_2 (see Table 1) is the rate of ATP degradation due to the presence of luciferin in the lumi-aggregometer used in the experiments. An additional term $\exp(-k_3 t)$ was also introduced in the model to fit the experimental data:

$$\frac{d[ATP]}{dt} = k_1[Ca^{2+}][PKC^*]e^{-k_3 t} - k_2[ATP], \qquad (4)$$

where $k_3 = 1.21 \times 10^{-1}\ s^{-1}$. The constant k_3 does not alter the physiological description of platelet exocytosis, but only allows a better fit. k_1, k_2 and k_3 were estimated using the method of least squares.[31] A comparison between experimental (blue) and simulated (red) ATP secretion curves is given in Fig. 4E.

4. Conclusions

We developed a kinetic model of PAR1 signaling in human platelets. The ODE model is populated with 60 equations and is fully based on available experimental data and previous computational models. Because of the inherent complexity of the problem, our model does not account explicitly for all the cellular mechanisms that drive platelet aggregation, but it incorporates only the major components affecting platelet activity. Nonetheless, the kinetic constants are carefully chosen to consider the effect of the omitted signaling components. In fact, a fully-detailed model of platelet signaling would be both unrealizable, due to the lack of experimental information, and computationally untreatable, because of the large number of parameters involved. Although far from being exhaustive, the current model is able to reproduce dose responses and time-courses of Ca^{2+}, PIP2, Rap1, GPIIbIIIa and ATP.

A recent experimental study demonstrated the link between PAR1-mediated formation of a stable platelet aggregate, persistent Rap1 activation, activation of PI-kinases, and signaling through PLD.[21] Although in this study we refrain from seeking an explicit computational link between simulated GPIIbIIIa activation and platelet aggregation data (not shown here), due to the fact that aggregation is also regulated by extracellular components (*e.g.* fibrin), our model still constitutes a valuable computational tool useful to study known cellular mechanisms and predict novel signaling pathways. For instance, one could easily perform a computational knockout experiment by setting to zero the concentration of one of the metabolites and study its effect on integrin activation. Similarly, the model could offer a study platform for performing inhibition assays. In fact, one could simulate the platelet behavior when PI5K is inhibited (*i.e.* PIP2 levels are decreased) by reducing the value of the constant A in eqn (1). Analogously, we showed how Rap1 attenuated responses in platelets treated with Akt X could be studied by tuning the output of the module that regulates Rap1 activation by Akt.

It is well known that the expression of activated GPIIbIIIa is increased in patients referred for coronary artery stenting or angioplasty.[10] The model could play an important role in identifying those metabolites that affect integrin expression in stimulated platelets. An in-depth study of these components may lead to the development of specific inhibitors with reduced side effects. For instance, the model emphasized the importance of PLD, PA and Akt signaling in platelet activity, all of which could be treated as potential therapeutic targets.

Although thrombotic events have a significant genetic component, there is little doubt that thrombosis can be the resulting effect of the abnormal interaction of the many components that regulate platelet activity. The model can offer a picture of the biological complexity of the platelet to help identify the genes or metabolites whose abnormal activity could lead to thrombosis. In fact, computational modeling allows the study of the role of variation in multiple genes simultaneously providing a very powerful means of study.

Biological networks are often populated with a myriad of metabolites and intricate pathways, making it difficult to model them. In this work we proposed a simple method to reduce the complexity of the system by lowering the number of unknown parameters. The method consisted in subdividing the whole signaling network into functional sub-networks or modules that share input and output signals. The modules were defined on the basis of their function and on the basis of the topology of the ODE pseudo-coefficient matrix. The number of unknown parameters was then reduced accordingly. Both the full and the reduced kinetic models were shown to qualitatively reproduce the experimental data. A fully-detailed description of the method and a sensitivity analysis study for the system parameters will be the object of a future work. Finally, we stress that kinetic parameters and concentrations are often difficult to measure. The values used in the simulations were chosen to fit the experimental data and can only be considered rough estimations of the real values. ODE models are, in fact, a simplification of the reality where some of the enzymes are membrane-bound and not freely diffusible and

some are found in larger complexes that locally control their activity. Compartimentation of diffusible molecules by degradative enzymes is also not captured by this simple model.

Acknowledgements

We are grateful to Nancy Colowick, Willie Hudson and Drs Alex Brown and Anita Preininger for useful discussions.

References

1 http://www.americanheart.org.
2 http://www.who.int.
3 P. C. Elwood, S. Renaud, D. S. Sharp, A. D. Beswick, J. R. O'Brien and J. W. Yarnell, *Circulation*, 1991, **83**, 38–44.
4 A. D. Michelson, *Platelets*, Academic Press, 2007.
5 S. R. Coughlin, *Nature*, 2000, **407**, 258–264.
6 L. K. Jennings, *Thromb. Haemostasis*, 2009, **102**, 248–257.
7 Y. Z. Xiang, Y. Xia, X. M. Gao, H. C. Shang, L. Y. Kang and B. L. Zhang, *Drugs*, 2008, **68**, 1647–1664.
8 B. E. Kehrel, *Haemostaseologie (Stuttgart, Ger.)*, 2008, **28**, 289–298.
9 C. J. Knight, M. Panesar, D. J. Wilson, N. A. Chronos, D. Patel, K. Fox and A. H. Goodall, *Circulation*, 1997, **95**, 125–132.
10 P. A. Gurbel and K. P. Bliden, *Thromb. Res.*, 2003, **112**, 9–12.
11 D. Andreucci, P. Bisegna, G. Caruso, H. E. Hamm and E. DiBenedetto, *Biophys. J.*, 2003, **85**, 1358–1376.
12 S. S. Andrews and A. P. Arkin, *Curr. Biol.*, 2006, **16**, R523–R527.
13 B. N. Kholodenko, O. V. Demin, G. Moehren and J. B. Hoek, *J. Biol. Chem.*, 1999, **274**, 30169–30181.
14 S. J. Bornheimer, M. R. Maurya, M. G. Farquhar and S. Subramaniam, *Proc. Natl. Acad. Sci. U. S. A.*, 2004, **101**, 15899–15904.
15 K. Sachs, O. Perez, D. Pe'er, D. A. Lauffenburger and G. P. Nolan, *Science*, 2005, **308**, 523–529.
16 K. A. Janes and M. B. Yaffe, *Nat. Rev. Mol. Cell Biol.*, 2006, **7**, 820–828.
17 J. E. Purvis, M. S. Chatterjee, L. F. Brass and S. L. Diamond, *Blood*, 2008, **112**, 4069–4079.
18 J. E. Purvis, R. Radhakrishnan and S. L. Diamond, *PLoS Comput. Biol.*, 2009, **5**, 1.
19 M. H. Fukami and H. Holmsen, *Eur. J. Biochem.*, 1995, **228**, 579–586.
20 L. Covic, A. L. Gresser and A. Kuliopulos, *Biochemistry*, 2000, **39**, 5458–5467.
21 M. Holinstat, A. M. Preininger, S. B. Milne, W. J. Hudson, H. A. Brown and H. E. Hamm, *Mol. Pharmacol.*, 2009, **76**, 301–313.
22 B. Voss, J. N. McLaughlin, M. Holinstat, R. Zent and H. E. Hamm, *Mol. Pharmacol.*, 2007, **71**, 1399–1406.
23 M. Holinstat, B. Voss, M. L. Bilodeau and H. E. Hamm, *Mol. Pharmacol.*, 2007, **71**, 686–694.
24 M. Holinstat, B. Voss, M. L. Bilodeau, J. N. McLaughlin, J. Cleator and H. E. Hamm, *J. Biol. Chem.*, 2006, **281**, 26665–26674.
25 Z. Zi, K.-H. Cho, M.-H. Sung, X. Xia, J. Zheng and Z. Sun, *FEBS Lett.*, 2005, **579**, 1101.
26 K.-H. Cho, S.-Y. Shin, W. Kolch and O. Wolkenhauer, *Simulation*, 2003, **79**, 726.
27 P. K. Dhar, H. Zhu and S. K. Mishra, *IEEE Trans. Nanobioscience*, 2004, **3**, 144–152.
28 U. S. Bhalla and R. Iyengar, *Science*, 1999, **283**, 381–387.
29 J. N. McLaughlin, L. Shen, M. Holinstat, J. D. Brooks, E. DiBenedetto and H. E. Hamm, *J. Biol. Chem.*, 2005, **280**, 25048–25059.
30 http://doqcs.ncbs.res.in/.
31 R. W. Shonkwiler and J. Herod, *Mathematical Biology. An introduction with Maple and Matlab*, Springer, 2009.
32 G. W. D. Young and J. Keizer, *Proc. Natl. Acad. Sci. U. S. A.*, 1992, **89**, 9895–9899.
33 S. E. Rittenhouse, *Proc. Natl. Acad. Sci. U. S. A.*, 1983, **80**, 5417–5420.
34 J. H. Exton, *Biochim. Biophys. Acta*, 1999, **1439**, 121–133.
35 G. M. Jenkins and M. A. Frohman, *Cell. Mol. Life Sci.*, 2005, **62**, 2305–2316.
36 L. G. Henage, J. H. Exton and H. A. Brown, *J. Biol. Chem.*, 2006, **281**, 3408–3417.
37 H. A. Brown, L. G. Henage, A. M. Preininger, Y. Xiang and J. H. Exton, *Methods Enzymol.*, 2007, **434**, 49–87.
38 S. Cockcroft, *Biochim. Biophys. Acta*, 2009, **1791**, 905–912.
39 Y. Kanaho, K. Nakayama, M. A. Frohman and T. Yokozeki, *Methods in Enzymology*, Elsevier, 2007, ch. 9, pp. 155–169.
40 H. Gong, B. S. P. Flevaris, C. Chow, S. C. Lam, T. A. Voyno-Yasenetskaya, T. Kozasa and X. Du, *Science*, 2010, **327**, 340–343.
41 K. Burridge and M. Chrzanowska-Wodnicka, *Annu. Rev. Cell Dev. Biol.*, 1996, **12**, 463–518.
42 J. R. Crittenden, W. Bergmeier, Y. Zhang, C. L. Piffath, Y. Liang, D. D. Wagner, D. E. Housman and A. M. Graybiel, *Nat. Med. (N. Y.)*, 2004, **10**, 982–986.
43 L. Stefanini, R. C. Roden and W. Bergmeier, *Blood*, 2009, **114**, 2506–2514.
44 J. Han, C. J. Lim, N. Watanabe, A. Soriani, B. Ratnikov, D. A. Calderwood, W. Puzon-McLaughlin, E. M. Lafuente, V. A. Boussiotis, S. J. Shattil and M. H. Ginsberg, *Curr. Biol.*, 2006, **16**, 1796–1806.
45 A. Banno and M. H. Ginsberg, *Biochem. Soc. Trans.*, 2008, **36**, 229–234.
46 S. J. Shattil, C. Kim and M. H. Ginsberg, *Nat. Rev. Mol. Cell Biol.*, 2010, **11**, 288–300.
47 L. Lian, Y. Wang, J. Draznin, D. Eslin, J. S. Bennett, M. Poncz, D. Wu and C. S. Abrams, *Blood*, 2005, **106**, 110–117.
48 P. Blair and R. Flaumenhaft, *Blood Rev.*, 2009, **23**, 177–189.
49 G. L. Reed, *Semin. Thromb. Hemostasis.*, 2004, **30**, 441–450.
50 S. M. King and G. L. Reed, *Semin. Cell Dev. Biol.*, 2002, **13**, 293–302.
51 G. L. Reed, M. L. Fitzgerald and J. Polgar, *Blood*, 2000, **96**, 3334–3342.
52 T. D. Schraw, P. P. Lemons, W. L. Dean and S. W. Whiteheart, *Biochem. J.*, 2003, **374**, 207–217.
53 R. Flaumenhaft, *Arterioscler., Thromb., Vasc. Biol.*, 2003, **23**, 1152–1160.
54 J. W. Barclay, T. J. Craig, R. J. Fisher, L. F. Ciufo, G. J. Evans, A. Morgan and R. D. Burgoyne, *J. Biol. Chem.*, 2003, **278**, 10538–10545.
55 A. Saltelli, K. Chan and M. Scott, *Sensitivity Analysis*, John Wiley & Sons Ltd, 2000 .
56 H. S. Ahn, C. Foster, G. Boykow, L. Arik, A. Smith-Torhan, D. Hesk and M. Chatterjee, *Mol. Pharmacol.*, 1997, **51**, 350–356.
57 H. Zhong, S. M. Wade, P. J. Woolf, J. J. Linderman, J. R. Traynor and R. R. Neubig, *J. Biol. Chem.*, 2003, **278**, 7278–7284.
58 G. H. Biddlecome, G. Berstein and E. M. Ross, *J. Biol. Chem.*, 1996, **271**, 7999–8007.
59 S. Mukhopadhyay and E. M. Ross, *Proc. Natl. Acad. Sci. U. S. A.*, 1999, **96**, 9539–9544.
60 E. M. Ross and T. M. Wilkie, *Annu. Rev. Biochem.*, 2000, **69**, 795–827.
61 J. L. Blank, K. A. Brattain and J. H. Exton, *J. Biol. Chem.*, 1992, **267**, 23069–23075.
62 G. Lemon, W. G. Gibson and M. R. Bennett, *J. Theor. Biol.*, 2003, **223**, 93–111.
63 T. Kozasa, X. Jiang, M. J. Hart, P. M. Sternweis, W. D. Singer, A. G. Gilman, G. Bollag and P. C. Sternweis, *Science*, 1998, **1998**, 2109–2111.
64 W. D. Singer, R. T. Miller and P. C. Sternweis, *J. Biol. Chem.*, 1994, **269**, 19796–19802.
65 K. Yamamoto, J. Kondo, T. Hishida, Y. Teranishi and Y. Takai, *J. Biol. Chem.*, 1988, **263**, 9926–9932.
66 D. E. Coleman, A. M. Berghuis, E. Lee, M. E. Linder, A. G. Gilman and S. R. Sprang, *Science*, 1999, **265**, 1405–1412.
67 P. A. O. Weernink, M. Schmidt and K. H. Jakobs, *Eur. J. Pharmacol.*, 2004, **500**, 87–99.
68 M. Duvernay, private communication.
69 C. Heinemann, L. von Ruden, R. H. Chow and E. Neher, *Pflugers Arch.*, 1993, **424**, 105–112.